

2 min

NASA TECHNICAL NOTE



NASA TN D-7493

NASA TN D-7493

(NASA-TN-D-7493) UPPER TROPOSPHERIC
DYNAMICS AS REFLECTED IN NIMBUS-4 THIR
6.7 MICRON DATA (NASA) 30 P HC \$3.00

CSCL 04A

N74-12169

Unclassified
23751

B1/13



UPPER TROPOSPHERIC DYNAMICS AS REFLECTED IN NIMBUS-4 THIR 6.7- μ m DATA

by Edward B. Rodgers, Vincent V. Salomonson,
and H. Lee Kyle

Goddard Space Flight Center
Greenbelt, Md. 20771

NATIONAL AERONAUTICS AND SPACE ADMINISTRATION • WASHINGTON, D. C. • DECEMBER 1973

1. Report No. NASA TN D-7493	2. Government Accession No.	3. Recipient's Catalog No.	
4. Title and Subtitle Upper Tropospheric Dynamics as Reflected in Nimbus-4 THIR 6.7- μ m Data		5. Report Date December 1973	6. Performing Organization Code 650
7. Author(s) Edward B. Rodgers, Vincent V. Salomonson, and H. Lee Kyle		8. Performing Organization Report No. G-7404	
9. Performing Organization Name and Address Goddard Space Flight Center Greenbelt, Maryland 20771		10. Work Unit No. 039-23-01-01	11. Contract or Grant No.
12. Sponsoring Agency Name and Address National Aeronautics and Space Administration Washington, D. C. 20546		13. Type of Report and Period Covered Technical Note	
14. Sponsoring Agency Code			
15. Supplementary Notes			
16. Abstract In order to determine if a quantifiable relationship exists between the 6.7- μ m radiometric patterns observed by the Nimbus-4 temperature-humidity infrared radiometer (THIR) and tropospheric dynamics, a 10-level diagnostic model is employed. The model is used to show the spatial and temporal relationships existing between radiometrically observed water vapor patterns and conventionally derived water vapor patterns, and to examine the upper and middle tropospheric water vapor budget and associated dynamics in order to assess the causes behind the spatially-and temporally-varying water vapor radiometric patterns. A particular situation involving a confluent trough located to the lee of the Rockies over the Central United States is examined. The THIR observations over the trough extend from 0538 GMT on April 30, 1970, to 1850 GMT on May 1, 1970, in approximately 12-hr increments. They reveal a tongue of warm equivalent blackbody temperature (T_{BB}) greater than 250K that advanced around and ahead of the trough. The movement of this warm tongue implies significant changes in the upper and middle tropospheric dynamics that characterize the different stages of the trough's life cycle.			
17. Key Words (Selected by Author(s)) Geophysics; Meteorology; Physics, general; Space Sciences		18. Distribution Statement Unclassified—Unlimited	
19. Security Classif. (of this report) Unclassified	20. Security Classif. (of this page) Unclassified	21. No. of Pages 26	22. Price* Domestic, \$3.00 Foreign, \$5.50

*For sale by the National Technical Information Service, Springfield, Virginia 22151.

CONTENTS

	<i>Page</i>
ABSTRACT	i
INTRODUCTION	1
DATA SOURCES	2
CASE STUDY	6
RESULTS	10
CONCLUSIONS	23
ACKNOWLEDGMENTS	23
REFERENCES	25
SOURCES	26

UPPER TROPOSPHERIC DYNAMICS AS REFLECTED IN NIMBUS-4 THIR 6.7- μ m DATA

Edward B. Rodgers

Environmental Research and Technology, Inc.

Vincent V. Salomonson and H. Lee Kyle

Goddard Space Flight Center

INTRODUCTION

It is known that the distribution of tropospheric water vapor is highly dependent upon the tropospheric dynamics associated with the circulation features in the free atmosphere (Reference 1). It is also known that when water vapor condenses, cloud patterns occur that are a function of atmospheric dynamics. In some instances, water vapor in an atmospheric volume is conserved and can be used as a tracer to delineate tropospheric dynamics. For example, a homogeneous air mass that has little or no entrainment can be considered to conserve its water vapor if there is no condensation and evaporation and if the air mass is above the turbulent mixing processes near the ground (Reference 2). Such conditions can be realized in cloud-free areas of the middle and upper troposphere, and thus, by monitoring water vapor through remote sensing, important details should be revealed about the tropospheric dynamics in these regions.

Observations of water vapor in the troposphere have been successfully accomplished through the use of satellites. As early as the television and infrared observation satellites (TIROS), extensive quantitative studies were made by Moller and Raschke (Reference 3), Allison and Warnecke (Reference 4), Raschke and Bandeen (Reference 5), and Fritz and Rao (Reference 6) to derive global upper tropospheric relative humidity from radiometric observations in the 6.0- to 6.5 μ m water vapor spectrum. Later, Smith (Reference 7), Smith and Howell (Reference 8), and Hanel and Conrath (Reference 9), derived vertical profiles of relative humidity and precipitable water from the infrared spectrometers onboard Nimbus meteorological satellites. However, the emphasis was on atmosphere moisture measurement, not on the relationship of moisture to atmospheric dynamics. Studies in relating spatially- and temporally-varying patterns derived from water-vapor radiometric data to the location and extent of atmospheric dynamics were made by Nordberg et al. (Reference 10), Beran et al. (Reference 11), Martin and Salomonson (Reference 12), Steranka et al. (Reference 13), Holub and Shenk (Reference 14), and Allison et al. (Reference 15), but such relationships were qualitative or semiquantitative. In attempting to study tropospheric dynamics through the use of water vapor patterns observed from a satellite, a diagnostic study should be made, relating the water vapor radiometric imagery to tropospheric dynamics derived from concurrent and independent conventional

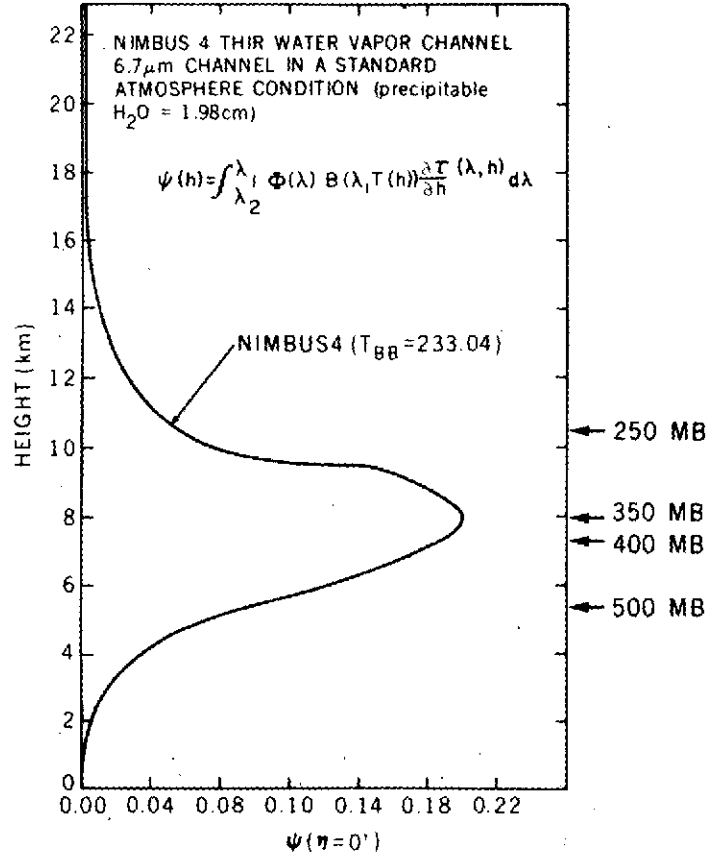
meteorological data. Once this relationship is understood, then water vapor radiometric data may be utilized more effectively to study tropospheric processes.

It is the purpose of this document to contribute to an understanding of such processes through a quantitative examination of a representative meteorological situation. The overall approach was first, to show the spatial and temporal relationships existing between the radiometrically observed water vapor patterns and the conventionally derived water vapor patterns and, secondly, to explain the causes behind the spatially- and temporally-varying water vapor radiometric patterns through an examination of the upper and middle tropospheric water vapor budget and associated dynamics. This provided a basis from which to evaluate more definitively the use of the radiometric 6.7- μm observations for inferring tropospheric dynamics.

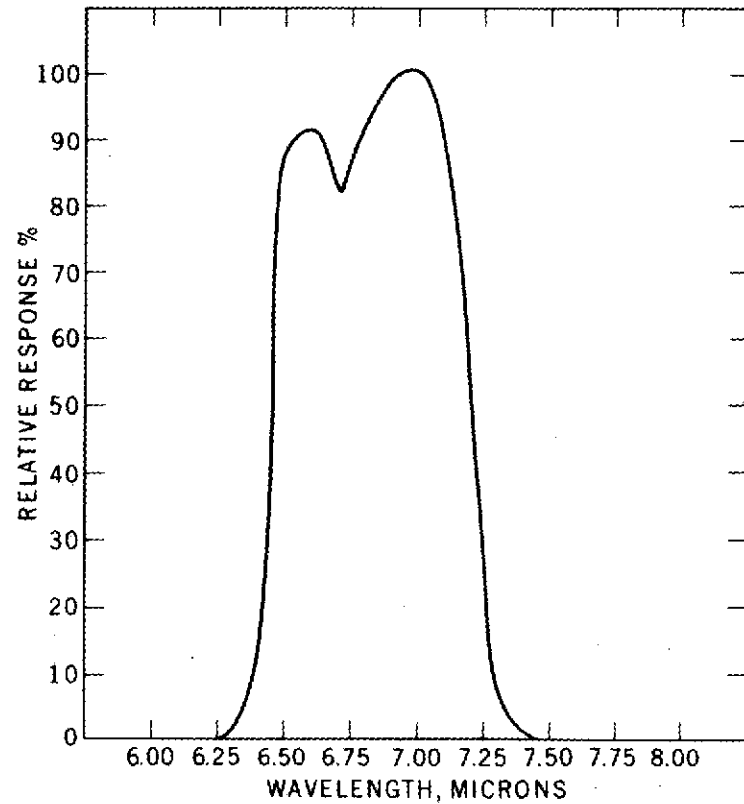
DATA SOURCES

The infrared radiometric water vapor data used in this study was acquired from the temperature-humidity infrared radiometer (THIR) experiment flown aboard the Nimbus-4 meteorological satellite. This high-resolution scanning radiometer contained two channels: a 10.5- to 12.5- μm "window" channel that provided day and night cloud-top or surface temperature with a ground resolution of 8 km at the subsatellite point, and a 6.4- to 7.2- μm "water vapor" channel that senses integrated moisture content for the upper troposphere and stratosphere with a ground resolution of 22 km at the subsatellite point. Figure 1(a) shows the contribution function curve for the water vapor channel based upon a standard atmosphere, and demonstrates that the emission from this given atmosphere is largely from a layer between 250 mbar to 500 mbar with the peak contribution emitting from about 350 mbar. Figure 1(b) depicts the spectral response for the water vapor channel and shows that the maximum response is approximately at 6.9 μm . In cloud-free areas the height of this peak contribution is more dependent upon the variation of moisture content within a column than the temperature variation of the column (Reference 11). Thus, the drier the column the lower the height of the peak contribution. This results in the column emitting at a higher weighted-mean equivalent blackbody temperature (T_{BB}). On the other hand, the more moist the column, the higher the height of the peak contribution, resulting in a lower T_{BB} . When opaque clouds fill the field of view, the measured T_{BB} is mainly dependent upon the temperature of the top of the cloud and the moisture content in the column between the cloud top and the sensor. In the case of nonopaque clouds that fill the field of view or opaque clouds that do not fill the field of view, it is difficult to evaluate the T_{BB} . Analog data will show lighter shades of gray for cold T_{BB} and darker shades of gray for warm T_{BB} (Reference 16). Figure 2 illustrates the analog form of observations taken over the Central United States on April 30, 1970, at 1745 GMT for both the 6.7- μm water vapor channel and the 11.5- μm window channel.

In the derivation of dynamic parameters from independent conventional meteorological data, a 10-level diagnostic model described by Barr et al. (Reference 17) was used. The model obtains vertical motions on a three-dimensional array with a 22-by-16 lateral grid



(a)



(b)

Figure 1(a). Spectral response of the Nimbus-4 THIR, $6.7\mu\text{m}$ channel.

(b). A plot of the weighting function, which shows the atmospheric emission contribution at different heights versus the radiance observed for the same channel.

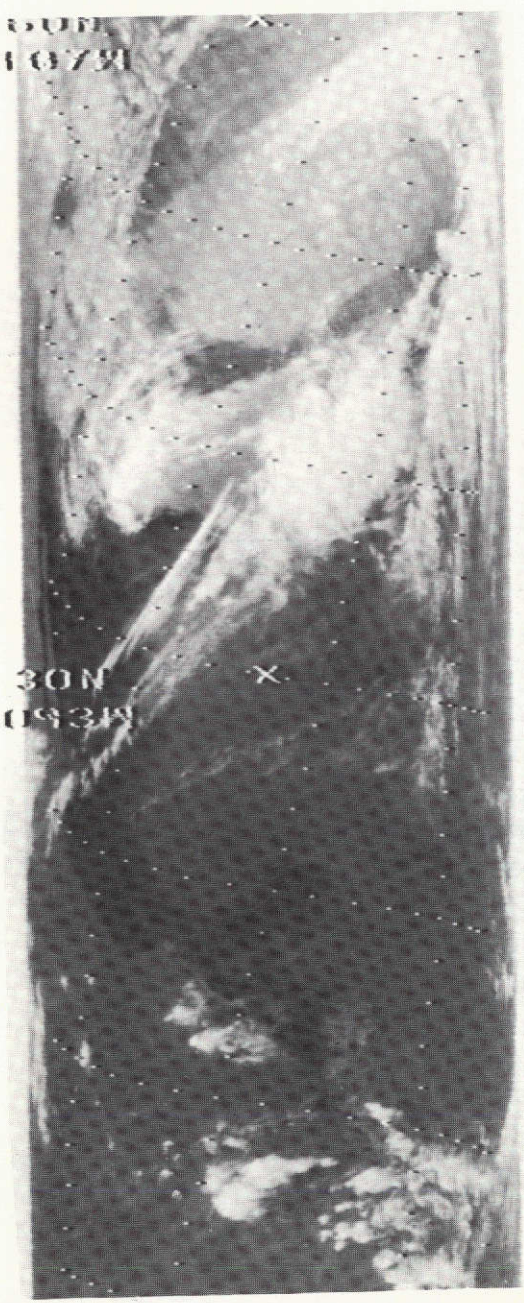
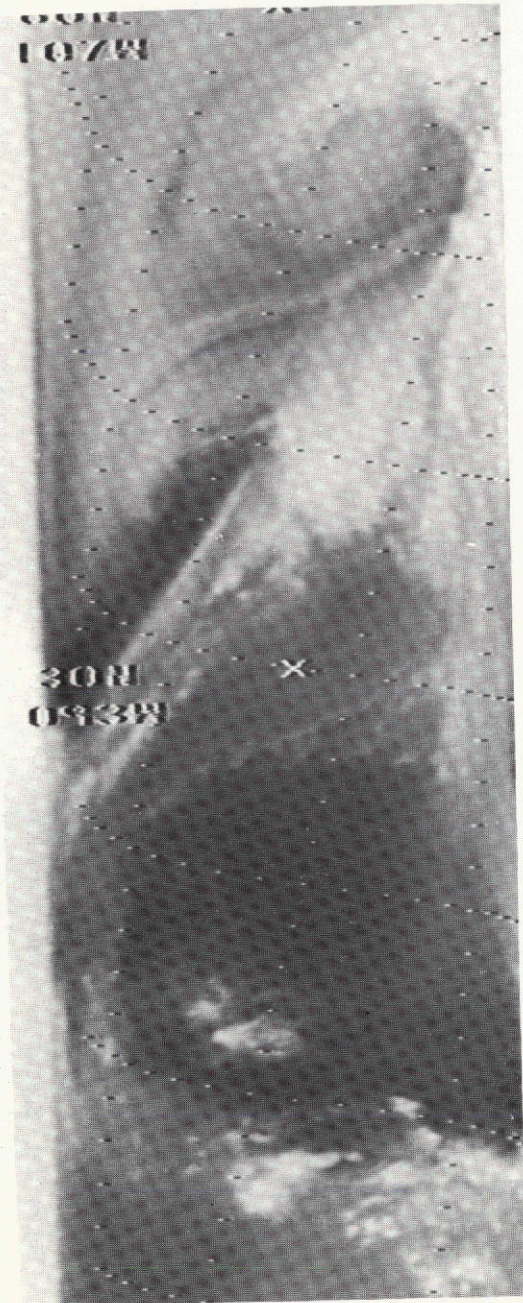


Figure 2. Photo facsimile film strip of the 6.7- μ m and 11.5- μ m data over the Central United States and the Gulf of Mexico during orbit 301 (D), April 30, 1970, at 1745 GMT.

spaced at 169-km intervals and a vertical spacing from 1000 mbar to 100 mbar at 100-mbar increments for an adiabatic atmosphere. Vertical motions were derived from the quasi-geostrophic omega equation

$$\nabla^2 \omega - \frac{f}{\sigma g} \frac{\partial^2 \omega}{\partial p^2} = \frac{-R}{\sigma gp} \nabla^2 (\bar{v} \cdot \nabla T) - \frac{f}{\sigma g} \frac{\partial(\bar{v} \cdot \nabla \zeta)}{\partial p} \quad (1)$$

where the Laplacian of horizontal temperature advection, $\frac{-R}{\sigma gp} \nabla^2 (\bar{v} \cdot \nabla T)$, and the vertical differential vorticity advection, $\frac{-f}{\sigma g} \frac{\partial(\bar{v} \cdot \nabla \zeta)}{\partial p}$, are employed as the two forcing terms.

The model assumes vertical motion to be zero at the top and at the sides of the three-dimensional array, and assumes no diabatic heating. Nonvanishing values of vertical motion are created by friction and topography at the bottom. The forcing terms are directly derived from fields of observed temperature and winds. This has an added advantage over models using fields of geopotential heights to solve for the forcing terms in that one differencing operator is eliminated, as in the vorticity term, and this enables the model to operate with less smoothing. Since smoothing is carried out at the expense of smaller scale details, the model can be used on a subsynoptic scale. The model is able to work on this scale because an overlapping triangle objective analysis technique is used.

This objective analysis scheme employs an array of overlapping triangles formed by three radiosonde observations in which meteorological parameters such as wind, temperature, geopotential heights, geostrophic winds, and temperature gradient, advection, and lapse rates are linearly averaged to the centroid of each triangle. These parameters are then smoothed in conjunction with actual radiosonde observations to the grid points. The advantage of the averaged meteorological triangle data is its ability to increase the spatial resolution by adding in more data in areas lacking radiosonde observation (Reference 18). The model is set up to derive many dynamics parameters such as geostrophic, relative, and absolute vorticity; horizontal divergence; u and v components of the real and geostrophic winds; temperature advection; and vorticity advection. Both forcing terms are derived together with the partitioned vertical motion that is induced by the individual forcing terms, and the total vertical motion, induced by the combined forcing terms. The lower boundary vertical motions induced by friction and topography are also calculated.

In order to determine how the tropospheric dynamics changes the water vapor distribution for an atmosphere that conserves its moisture, the model was revised so as to evaluate the local change of water vapor for the three-dimensional grid, assuming no evaporation and condensation. This local change can be expressed as

$$\frac{\partial q}{\partial t} = -\bar{v} \cdot \nabla q + q \frac{\partial \omega}{\partial p} - \frac{\partial \omega q}{\partial p} \quad (2)$$

where

$$\begin{aligned}\frac{\partial q}{\partial t} &= \text{local change of } q \\ -\bar{v} \cdot \nabla q &= \text{horizontal advection of } q \\ \left. \begin{aligned} \frac{q \frac{\partial \omega}{\partial p}}{\partial p} \\ - \frac{\partial \omega q}{\partial p} \end{aligned} \right\} &= -\omega \frac{\partial q}{\partial p} = \text{vertical advection of } q\end{aligned}$$

The model computes the horizontal as well as the vertical advection of specific humidity (Reference 1), and then algebraically adds the terms to obtain the local change of specific humidity.

CASE STUDY

In choosing a case study, consideration had to be given to three criteria: The choice of an upper troposphere synoptic circulation had to illustrate the relationship between the dynamics associated with the circulation and water vapor for an atmosphere for which water vapor was at least quasi-conservative. The location of the synoptic pattern had to be situated over a dense data area in order to employ the diagnostic model. And the monitoring of this synoptic system by remote sensor had to be continuous at least in 12-hr intervals in order to appreciate the temporal changing patterns seen in the T_{BB} observations.

Although there were several synoptic patterns that fulfilled the three criteria described above, a high amplitude trough situated to the lee of the Rockies over the Central United States was selected because it best illustrated large upper tropospheric dynamic variation attributable to its large meridional energy exchange characteristics. The preocclusion stage of the trough development was examined since it is during this stage that dry air often begins to invade the extratropical cyclone, eventually cutting off its moisture supply. It is this homogeneous, relatively conservative dry tongue feature (generally existing in association with clear skies) that will be examined in more detail. The geopotential pattern for the period 1200 GMT on April 30 to 1200 GMT on May 1, 1970, can be seen in Figure 3.

In this study the trough was monitored for 36 hr by the Nimbus-4 THIR water and window channels, from 0600 GMT on April 30, 1970, to 1800 GMT on May 1, 1970, in approximately 12-hr increments (Figures 4(a), (b), (c) and (d)). The diagnostic model quantitatively examined the air mass in three dimensions at approximately 6 hr before and after each satellite pass. Since the maximum emission detected from the 6.7- μ m water vapor channel comes principally from a layer extending from 500 to 250 mbar for a standard cloud-free atmosphere, most of the results presented will relate to the middle and upper troposphere.

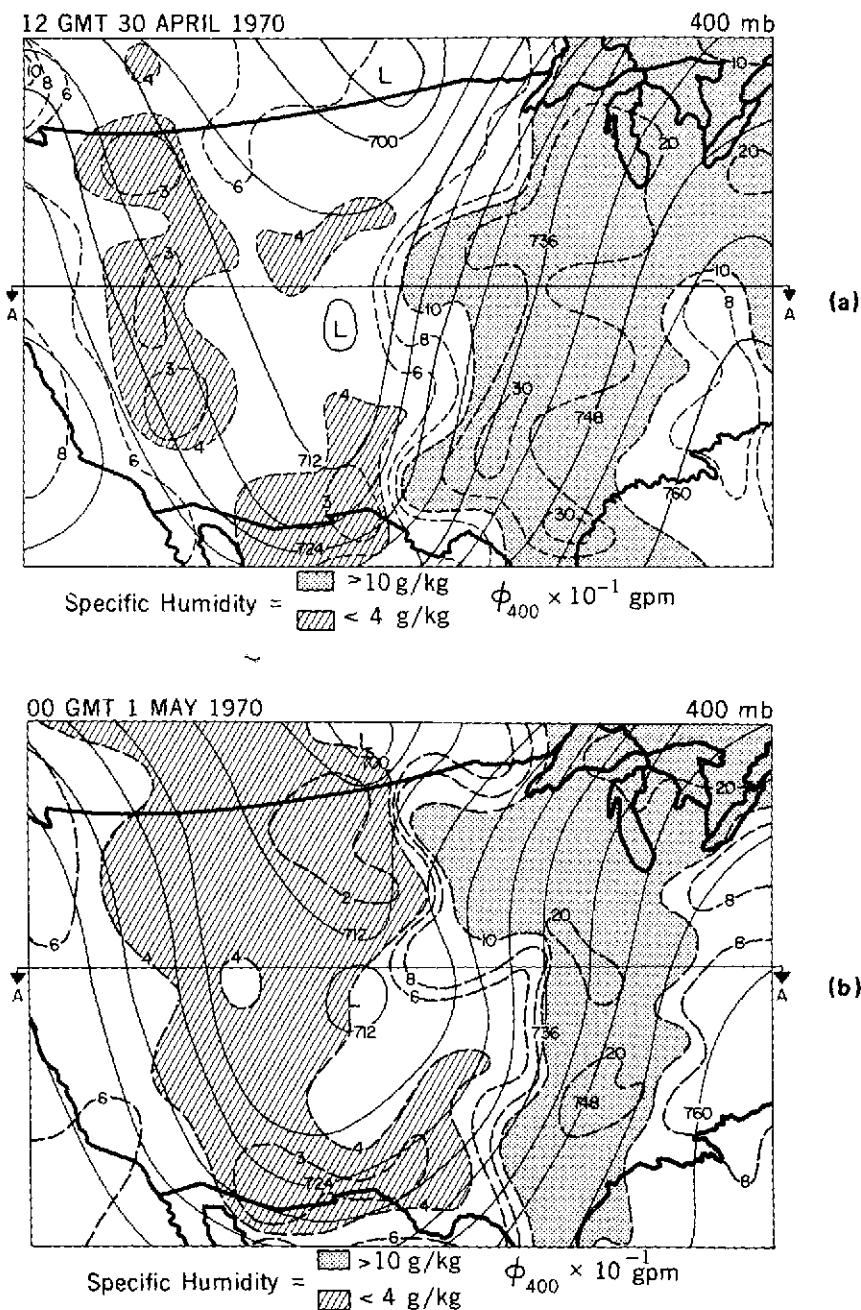


Figure 3. 400-mbar geopotential heights superimposed upon the 500-mbar specific humidity field for (a) 1200 GMT on April 30, and (b) 00 GMT on May 1, over the Central United States. Line A designates location of cross section A.

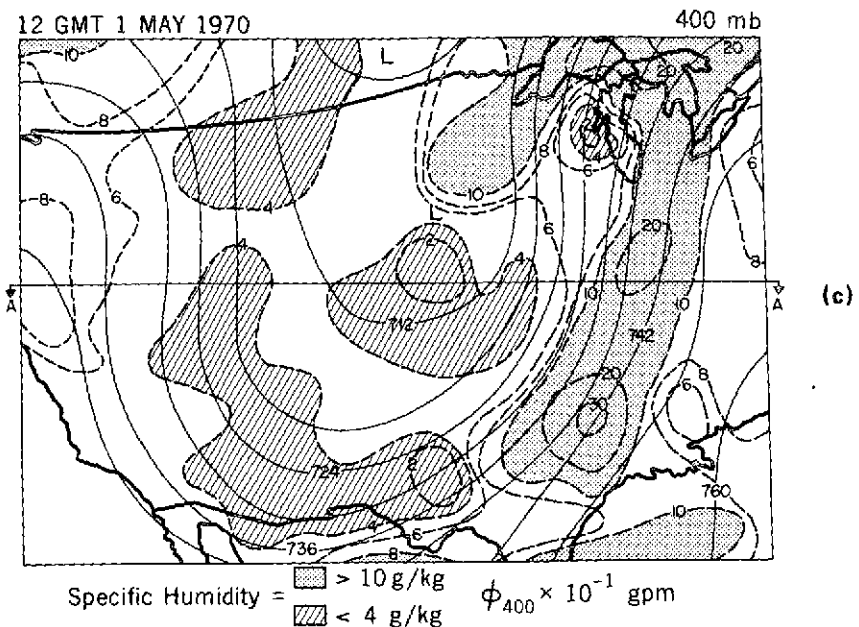


Figure 3. 400-mbar geopotential heights superimposed upon the 500-mbar specific humidity field for (c) 1200 GMT on May 1, 1970, over the Central United States. Line A designates location of cross section A.

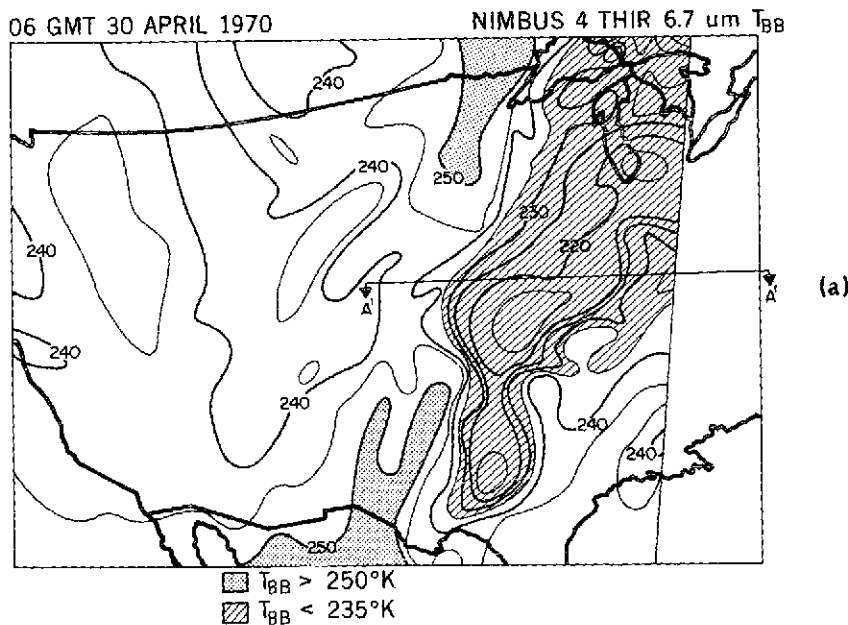


Figure 4. The field of equivalent blackbody temperature obtained from the Nimbus-4 THIR 6.7- μm channel digital data for (a) 0600 GMT on April 30, over the Central United States. Line A' designates location of cross section A'.

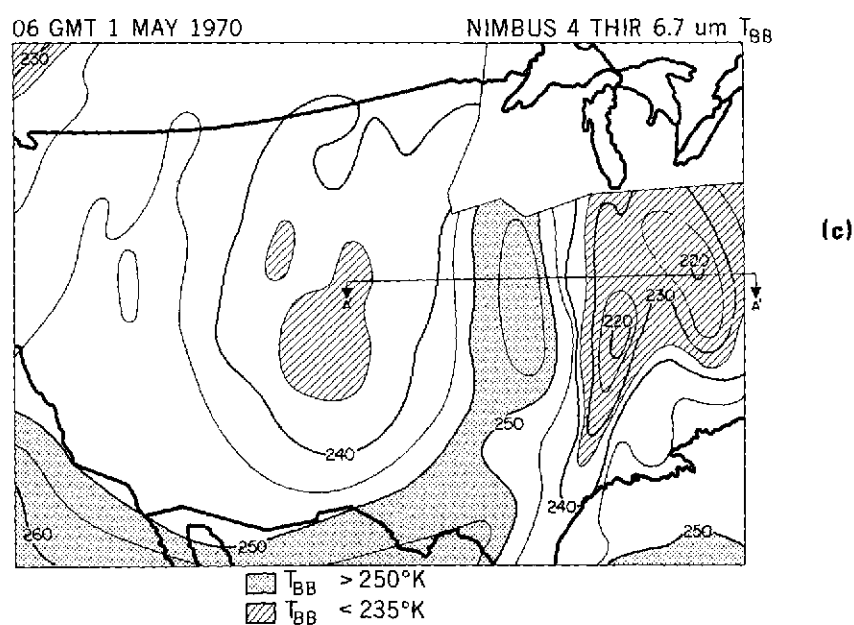
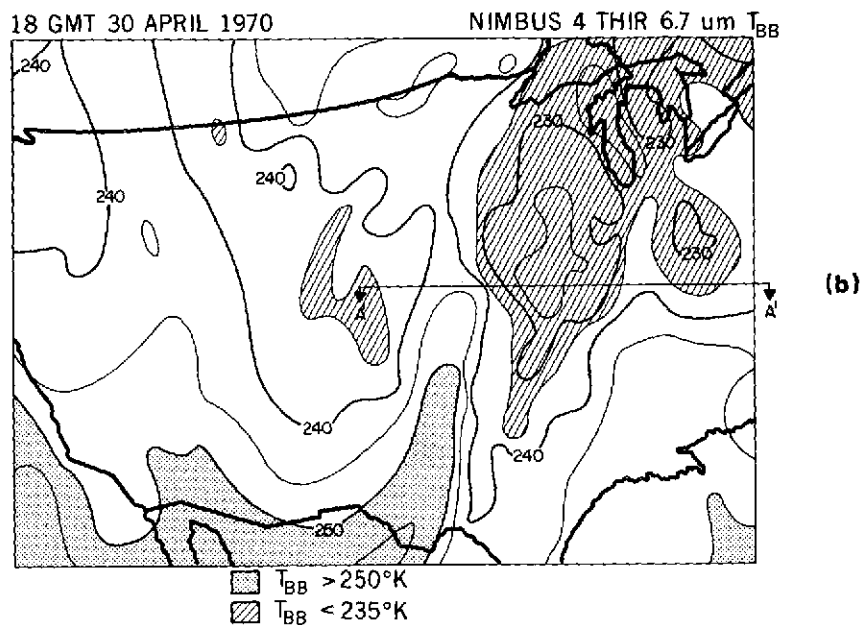


Figure 4. The field of equivalent blackbody temperature obtained from the Nimbus-4 THIR 6.7- μ m channel digital data for (b) 1800 GMT on April 30, and (c) 0600 GMT on May 1, over the Central United States. Line A' designates location of cross section A'.

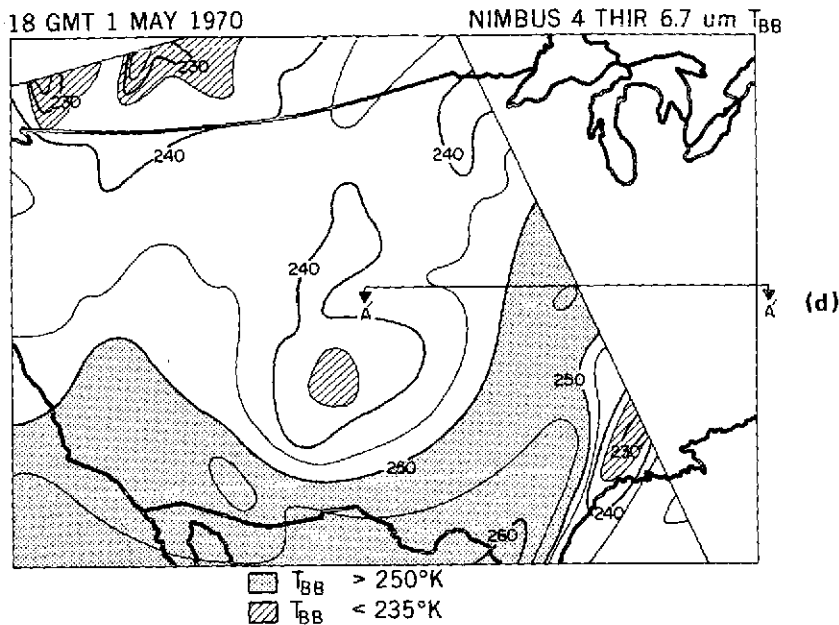


Figure 4. The field of equivalent blackbody temperature obtained from the Nimbus-4 THIR 6.7- μm channel digital data for (d) 1800 GMT on May 1, 1970, over the Central United States. Line A' designates location of cross section A'.

RESULTS

Spatial and Temporal Relationships Between Water Vapor Radiometric Imageries and Conventionally Derived Water Vapor Patterns

The first step in this quantitative evaluation of the water vapor radiometric data was to assess the spatial and temporal relationships between the radiometrically observed water vapor patterns and conventionally derived water vapor patterns.

The conventional water vapor data that was used consisted of specific humidity values observed by radiosondes at the 500-mbar level. The 500-mbar level was used since it is the closest standard level to the level of peak contribution in the 6.7- μm water vapor radiometric measurements for which radiosonde measurements are accurate and abundant. In Figures 3(a), (b), and (c), the dashed lines depict the 500-mbar specific humidity, while the solid lines depict 400-mbar geopotential heights for 1200 GMT on April 30, 00 GMT on May 1 and 1200 GMT on May 1, 1970. The pattern of particular interest is the area of dry air delineated by the isopleths of specific humidity for less than 4g/kg. At 1200 GMT on April 30, 1970, there were three such areas of dry air. One was to the south of the primary closed low seen over the Northern Plains, another was entering the southern section of the secondary closed low seen over Texas, and a third was entering the trough from the northwest Canadian region. Twelve hours later at 00 GMT on May 1, 1970, the

two areas to the south of each closed low expanded and were drier. The dry air seen at the base of the secondary closed low 12 hr previous had infiltrated further east and northwards displacing the moist air over the Mississippi Valley. The dry tongue entering the trough from Northwest Canada had also expanded and moved southeastward merging with the other two dry areas. At 1200 GMT on May 1, 1970, the dry tongue associated with the secondary closed low had progressed further north and eastward along the eastern part of the trough, subsequently displacing the more moist air over the Upper Mississippi Valley. The dry air that was seen entering from the northwest Canadian region had now moved into the southern section of the trough.

In assessing the spatial and temporal relationship between the conventionally derived and radiometrically observed water vapor patterns, the THIR 6.7- μ m water vapor data were then compared with the conventional water vapor patterns in cloud-free areas. The THIR 6.7- μ m water vapor imagery is seen in Figures 4(a), (b), (c), and (d), as derived from digitized 6.7- μ m THIR data provided on computer compatible magnetic tapes (Reference 16). Areas that were most likely cloud-free are delineated by T_{BB} that were greater than 250 K. Although the satellite pass was approximately 6 hr before or after radiosonde observation time, the spatial configuration of the water vapor radiometric data in cloud-free areas satisfactorily delineated the dry air observed in the conventional data. The best comparison was found between the tongue of dry air that was associated with the secondary closed low and the tongue of warm T_{BB} greater than 250 K. The tongue of T_{BB} greater than 250 K not only delineated the spatial configuration of the dry air but suggested a good relationship with the moving spatial patterns of dry air throughout the period as well. This tongue seen over Western Texas at 0600 GMT on April 30, 1970, progressed north and eastward during the next 24 hr, infiltrating much of the eastern section of the trough. The tongue followed the same path as that traversed by the dry tongue in the conventional data. However, the dry tongue seen in the conventional data that originated from the southern section of the primary closed low was not as well delineated by the T_{BB} patterns in the water vapor radiometric data, because of the advection of upper tropospheric opaque and semiopaque clouds. The area of upper tropospheric clouds is essentially depicted by an area of cold T_{BB} with values less than 240 K.

Relationship Between Upper Tropospheric Dynamics and the Spatial and Temporal Varying Water Vapor Radiometric Patterns

In evaluating the water vapor imagery an examination was made to study the effects of the dynamics upon the distribution of water vapor both in the middle and upper troposphere. To determine the water vapor budget, the local change of specific humidity was calculated for all internal points at 100-mbar increments in the diagnostic model array above 800 mbar, assuming no precipitation and little or no evaporation. This is a good assumption in cloud-free areas. The local change of specific humidity was evaluated by algebraically adding the horizontal advection to the two terms of the vertical advection of specific humidity seen on the right-hand side of Equation (2) (Reference 1). In delineating

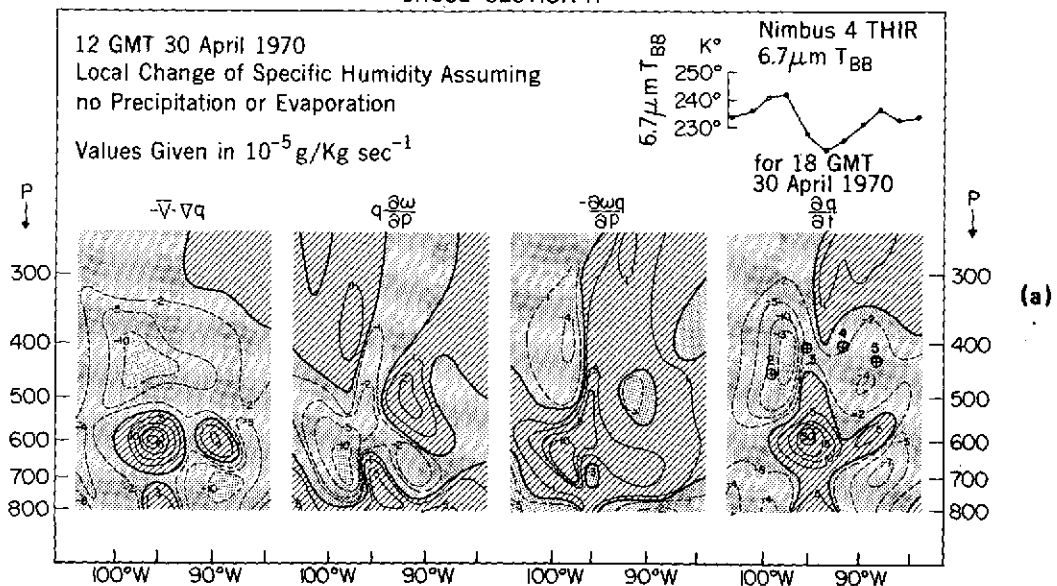
these calculations, cross sections showing the calculated values of each partitioned term as well as the total local change of specific humidity at 100-mbar increments within the column were made. Since it is impractical to show all cross sections across the grid, the choice was made to take one section across an area that showed the greatest change in T_{BB} in the water vapor radiometric data during the period. Such an area was located east of the trough over the Mississippi Valley, where a tongue of warm T_{BB} greater than 250 K was observed (Figures 4(a), (b), (c) and (d)) to advance northeastward from Texas to the Upper Mississippi Valley; the cross section is designated by A' in the figures. Figures 5(a), (b), and (c) depict cross section A' for 1200 GMT on April 30, 00 GMT on May 1, and 1200 GMT on May 1, 1970, respectively. The cross sections show the calculated partitioned term together with the total local change of specific humidity term for all 100-mbar levels between 800 and 250 mbar. Above the derived total local change of specific humidity is a T_{BB} trace extracted from the 6.7- μ m water vapor digital maps for the same intersection approximately 6 hr after the radiosonde observation time.

In examining these cross sections, attention is first given to the local change of specific humidity. At 1200 GMT on April 30, 1970, evidence of the influx of dry air seen upstream from the cross section is depicted by the loss of moisture of values as high as 13×10^{-5} g/kg/s between 400 and 500 mbar at approximately 97° W longitude. This decrease of upper tropospheric moisture is also evident in the T_{BB} , with the drying column reflecting temperatures as high as 242 K. The middle tropospheric drying observed to the east, however, is not reflected in the T_{BB} trace. Here, T_{BB} 's are representations of middle level clouds associated with high moisture influx at 95° W longitude in the middle troposphere. Twelve hours later at 00 GMT on May 1, 1970, in the western section of the cross section, the drier air has advected eastward to 95° W longitude, and shifted downward to the middle troposphere. This middle tropospheric drying is depicted quite well by the T_{BB} 's. The further drying and eastward extension of the column is illustrated by the 13-K increase in T_{BB} 's. Further east the decrease in T_{BB} in response to the clouds associated with the moisture influx is seen throughout the column at 92° W longitude. The local change of specific humidity calculation shows at 1200 GMT on May 1, 1970, that the whole column in the western section is continuing to dry but at a much slower rate. However, at 90° W longitude strong drying is again evident but only above 500 mbar. The T_{BB} pattern illustrates the further drying over the western section, but because of the loss of the data orbit, the decrease in specific humidity calculated in the eastern half could not be delineated.

Attention is now given to the partitioned terms in Equation (2) in order to understand the dynamical causes for the water vapor distribution. The magnitude of these lines are graphically explained in Figures 5(a), (b), and (c).

The drying that was evident in the middle troposphere near 97° W longitude at 1200 GMT on April 30, 1970, is maintained mostly by horizontal advection. The calculated values for this term of nearly -10^{-4} g/kg/s explains most of the variance in the total change of specific humidity. The vertical advection processes, quantitatively represented by the remaining partition terms in Equation (2) are seen to contribute no more than 30 percent

CROSS SECTION A



CROSS SECTION A'

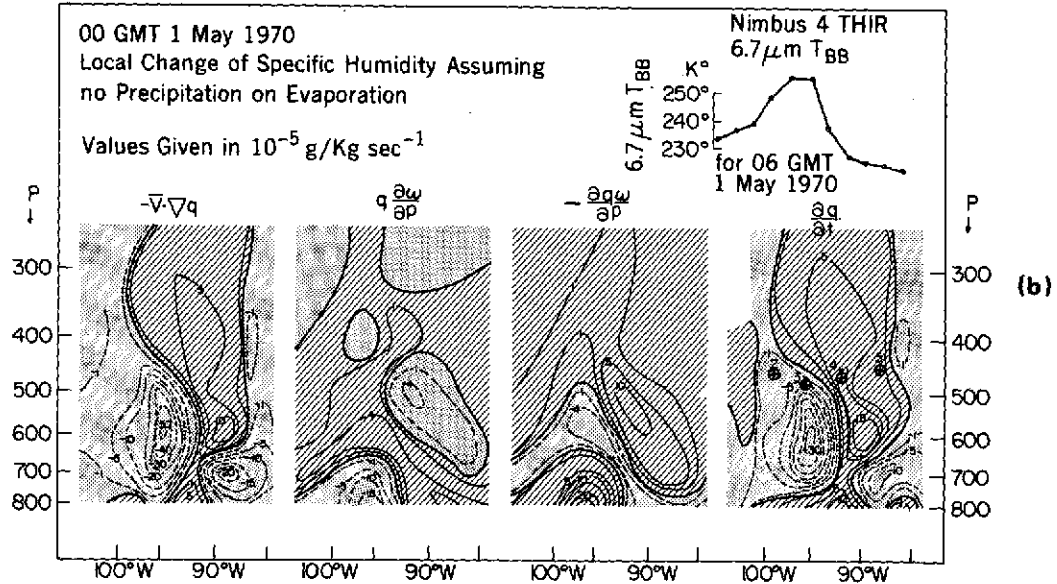


Figure 5. The calculations from the horizontal and vertical advection of specific humidity, and the local change of specific humidity along cross section A' between 800 and 300 mbar levels from (a) 1200 GMT on April 30, and (b) 00 GMT on May 1, data. Above the local change of specific humidity calculation is a trace of the $6.7\text{-}\mu\text{m}$ equivalent blackbody temperature obtained from along cross section A' 6 hours after the local change of specific humidity calculations. The cross within the circles labeled from 2 to 4 designate intersect of the parcels in trajectories 2 to 5.

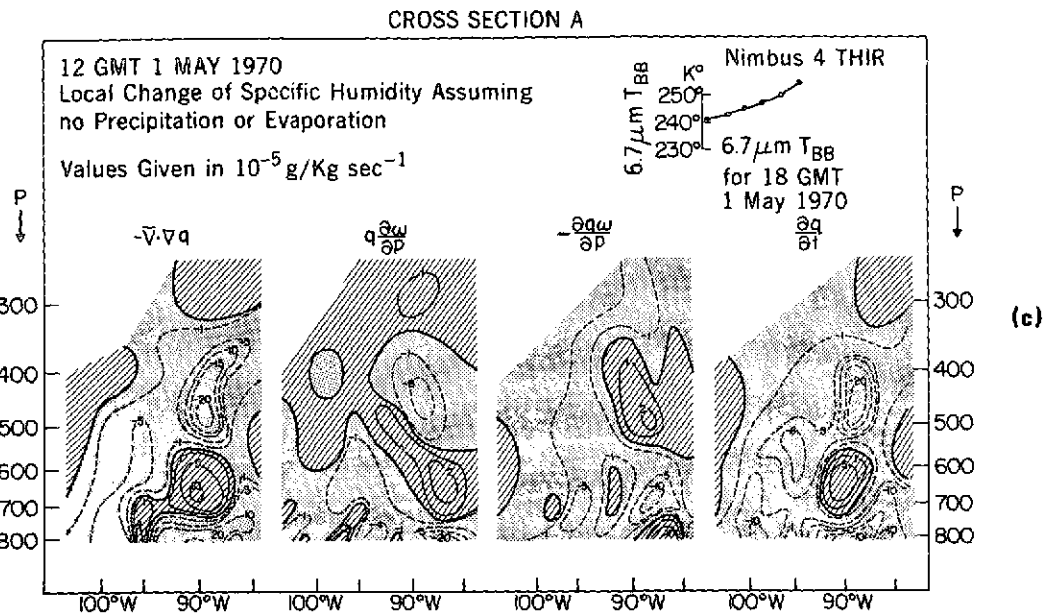


Figure 5. The calculations from the horizontal and vertical advection of specific humidity, and the local change of specific humidity along cross section A' between 800 and 300 mbar levels from (c) 1200 GMT on May 1, 1970 data. Above the local change of specific humidity calculation is a trace of the 6.7- μ m equivalent blackbody temperature obtained from along cross section A' 6 hours after the local change of specific humidity calculations.

to the total loss of specific humidity. At 00 GMT on May 1, 1970, the large loss of specific humidity at 600 mbar near 95° W longitude is strictly due to horizontal advection. However, the moisture increase seen at 92° W longitude throughout the column is maintained by horizontal as well as vertical advection processes. The loss of specific humidity seen throughout the column west of 93° W longitude, particularly between 400 to 500 mbar near 90° W longitude at 1200 GMT on May 1, 1970, is once again due to horizontal advection, with vertical advection processes contributing less than 30 percent to the total change in specific humidity.

The examination of the water vapor balance calculation for the given period has revealed two points. First, the distribution of water vapor within cross section A' was controlled mainly by horizontal advection processes, particularly in the upper and middle troposphere. Second, vertical advection processes were calculated to be small in the cross section area, nevertheless, they progressively aided in drying the lower levels upstream.

Although the cross section covered a limited sector of the array, the water vapor budget calculation did demonstrate the effects that the middle and upper tropospheric circulation had upon the distribution of water vapor and the fluctuations of T_{BB} in the water vapor radiometric data on a Eulerian frame of reference. However, to further demonstrate the

actual dynamics that caused the distribution of the upper and middle tropospheric water vapor and T_{BB} 's seen in the water vapor radiometric data, the Lagrangian approach using trajectories was employed to give a four-dimensional picture of these relationships.

In demonstrating these relationships, three-dimensional trajectories were used that were linearly interpolated at 3-hr intervals between radiosonde observation times (Reference 19). The three-dimensional trajectories that were initiated at the 450-mbar level intersected cross section A' at intermediate radiosonde times. The intersection of trajectories 2 through 5 were designated by a circled cross, to show that the parcels were passing into the page. The trajectories were also superimposed upon the intermediate 6.7- μ m radiometric data in order to better illustrate dynamically the water vapor radiometric pattern changes. Figure 6(a) shows five trajectories starting at 1200 GMT on April 30, 1970, at the 450-mbar level and ending at 00 GMT on May 1, 1970, that are superimposed upon the 1800 GMT 6.7- μ m radiometric data. Figure 6(b) shows five more trajectories starting at 00 GMT on May 1, 1970, at the 450-mbar level and ending at 1200 GMT on May 1, 1970, superimposed upon the 0600 GMT 6.7- μ m radiometric data. The trajectories were used to trace the upper tropospheric flow on both sides as well as within the warm tongue of T_{BB} that is being followed by remote sensing.

Although trajectory 1 does not traverse cross section A', it is important to mention it since it explains the discrepancy between the conventional and radiometric water vapor data seen previously. The ascending motion of the parcel of nearly 100 mbar in 12 hr seen during both the first and second 12-hr periods was strong enough to cool and condense the dry air observed upstream at lower levels to form the clouds delineated by the T_{BB} less than 235 K. Therefore, the dry air seen on the conventional data at 500 mbar was not seen here because of this upper tropospheric cloudiness.

During the first 12 hr, trajectories 3, 4, and 5 were constructed in order to explain the upper tropospheric dynamical contribution to the cloud mass seen in the cold T_{BB} of less than 235 K. Trajectory 3 depicts the parcel moving within the core of the polar jet as delineated from the large lateral displacements. As the parcel curved slightly cyclonically ahead of the trough with the jet, it was seen to rise nearly 50 mbar during the first 6 hr. Continued rapid ascending motion, as much as 50 mbar in 3 hr, was observed during the following 6 hr as the parcel moved into the ridge. Trajectory 4 reveals a parcel to the east of the jet core as delineated by smaller lateral displacements. Again large rising motion was observed in the order of 100 mbar during the 12-hr period. Even further east of the jet core, trajectory 5 reveals that air is also rising but at a lesser rate of only 40 mbar in 12 hr. All three of the trajectories reveal that the surface at 450 mbar east of the jet core is rising as it passes through cross section A' east of 96° W longitude. However, near the 400-mbar level where the trajectories intersect the cross section (Figure 5(a)), water vapor budget calculations show that there is a slight decrease of specific humidity in the region of the cross section due to the horizontal advection of drier air from upstream. The water vapor that is being brought into the cross section is from the vertical flux of water vapor from below. Thus, the cloudiness seen in the radiometric data is due to the condensing of this upward flux of moisture.

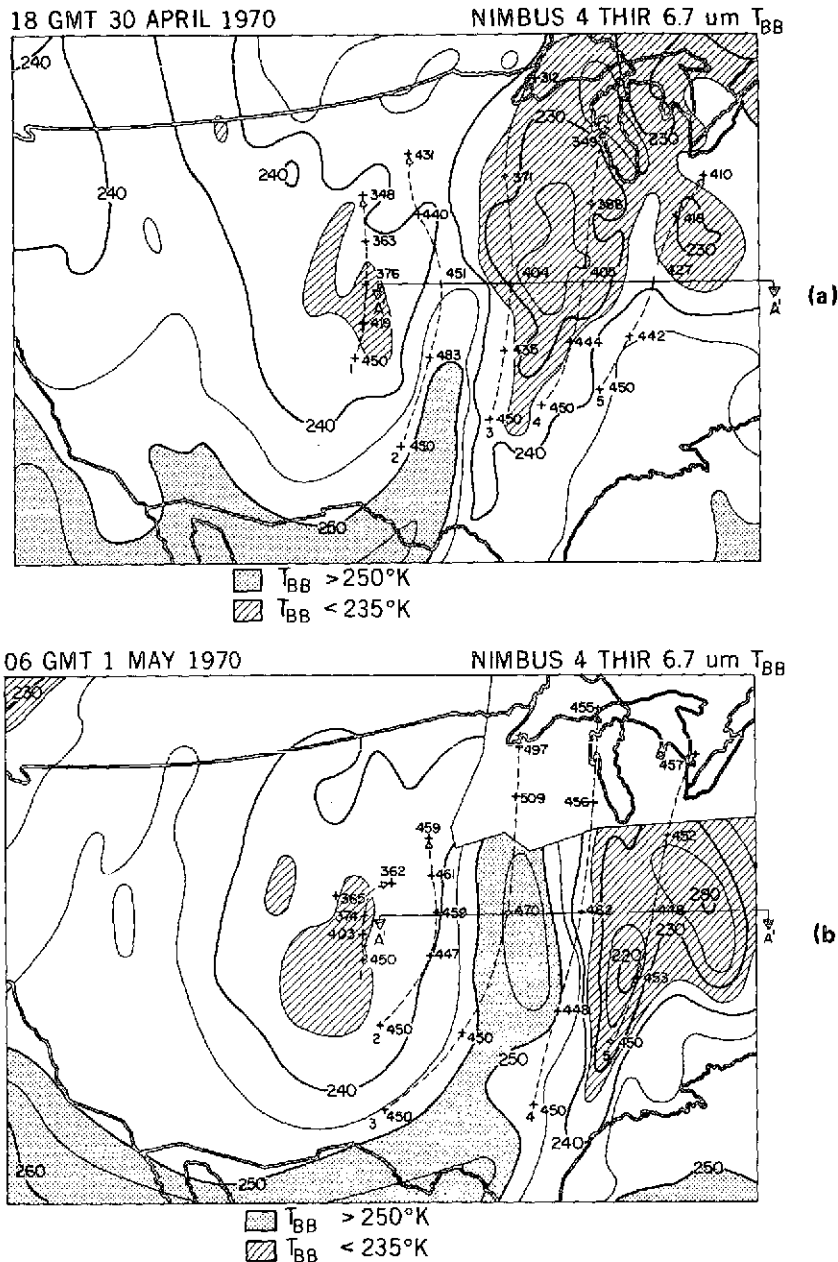


Figure 6(a). Three-dimensional trajectories between 1200 GMT on April 30, and 00 GMT on May 1, 1970, initiated at the 450-mbar level superimposed upon the 6.7- μ m equivalent blackbody temperatures for 1800 GMT on April 30, 1970. (b) Three-dimensional trajectories between 00 GMT on May 1, and 1200 GMT on May 1, 1970, initiated at the 450-mbar level superimposed upon the 6.7- μ m equivalent blackbody temperature for 0600 GMT on May 1, 1970. In both figures crosses represent the position of the parcels at 3-hour intervals, and the number to the side represents the pressure height. Line A' represents cross section A'.

The areas of most interest, as mentioned before, are the cloud-free areas depicted primarily by a warm tongue of T_{BB} 's greater than 250 K. Here trajectory 2 represents upper and middle tropospheric dynamics within this tongue. During the first 3 hr, air that moved ahead of the trough had descended 33 mbar, which corresponds quite well with the T_{BB} 's greater than 250 K. However, during the following 9 hr, the parcel ascended 50 mbar corresponding to cooler T_{BB} 's downstream. As the parcel moved through cross section A' (Figure 5(a)) it was revealed from the water vapor budget calculation that at the level in which the parcel intersected the cross section, approximately 450 mbar, the column was drying at the rate of 12×10^{-5} g/kg/s. As seen from the water vapor budget calculations and the trajectories, this drying was produced by horizontal advection of air upstream that had subsided during the previous 3 hr. Even though the parcel was ascending as it moved through the cross section, the parcel was drier than the ambient air in the cross section.

During the following 12 hr, from 00 GMT to 1200 GMT on May 1, 1970, the vigorous upper tropospheric ascending motion east of the jet had moved northeastward. Trajectory 4 depicts a parcel of air in the upper troposphere just east of the jet core that showed little vertical displacement. As the parcel moved into cross section A' (Figure 5(b)) near the 450-mbar level, it was advecting higher values of specific humidity at a rate of approximately 10^{-4} g/kg/s as seen in the water vapor budget calculations. Both the horizontal advection of moist air and the upward vertical advection go together to increase the moisture within this column. Trajectory 5 again shows very little vertical displacement of the parcel as it moved up the trough east of the jet core. However, as the parcel entered the cross section, water vapor budget calculations show that the column near 450 mbar was increasing in moisture. This is indicative of the horizontal advection of moisture produced by ascending air that was upstream 3 hr previously and the vertical upward flux of moisture within the column. This again aided in producing the upper tropospheric clouds seen in the water vapor radiometric data.

Trajectory 2 depicts the dynamics of the upper tropospheric circulation west of the jet core. As the parcel intersected the cross section (Figure 5(b)), the rate of drying was greater than 10^{-5} g/kg/s. As depicted by the water vapor budget calculation and trajectories, there was horizontal advection of dry air produced by moderate subsidence of nearly 12 mbar during the previous 3 hr.

Trajectory 3 again depicts the dynamics in the upper troposphere associated with the warm tongue of T_{BB} greater than 250 K. As seen by the vertical displacement of the parcel, air at the 450-mbar level moving with jet core has subsided approximately 60 mbar during the first 9 hr, which corresponds quite well with the warm tongue of T_{BB} greater than 250 K. As the parcel moves through the cross section A' (Figure 5(b)), it enters just above the level of maximum drying. However, the parcel is representative of all air parcels moving through the cross section in the middle tropospheric region. As shown in the water vapor budget calculations and trajectories, the middle tropospheric column was drying by three-dimensional advection. Horizontal advection of dry air produced by subsidence upstream

during the previous 6 hr and subsidence within the column combined to produce the warm tongue.

It is now apparent from the water vapor budget calculations and the three-dimensional trajectories which upper tropospheric dynamics had caused the water vapor distribution seen in the 6.7- μ m water vapor radiometric data. However, to go one step further in this quantitative analysis of the radiometric data, a synoptic evaluation will be made to determine the causes behind the upper tropospheric dynamics.

The upper tropospheric synoptic picture is best illustrated in Figures 7(a), (b), and (c). These figures that contain the 400-mbar geopotential heights and radiosonde wind observations, the 450-mbar vertical motion patterns, and the 500-mbar specific humidity isopleths, show the trough at 1200 GMT on April 30, 00 GMT on May 1, and 1200 GMT on May 1, 1970, during its preocclusion stage.

The area of particular interest, as stated previously, is the warm tongue of T_{BB} greater than 250 K seen in the water vapor radiometric data in Figures 5(a), (b), and (c) that was shown to be associated with the dry tongue of air seen in Figure 4. In synoptically explaining this dry tongue, Palmen and Newton (Reference 1) had shown that during the preocclusion stage of development of a trough the dry air seen advecting up ahead of the trough is part of the collapsing cold dome that had been in equilibrium during the earlier stages. To ascertain whether this trough was in the preocclusion stage, observations were made of the horizontal and vertical components of the wind during the period.

In Figures 7(a), (b), and (c), the jet maximum (winds greater than 45 mps) at the 400-mbar level is seen to be out ahead of the trough for the time period. This configuration is indicative of the preocclusion stage. Further evidence is seen in Figure 8 which depicts the partitioned as well as the total vertical motion plots at 550 mbar across the base of the trough delineated by line A in Figures 7(a), (b), and (c), for the three time periods. It is observed from the plots that the Laplacian of horizontal temperature advection becomes more of a dominating, forcing term later in the period. This is indicative of the preocclusion or confluent stage of the trough, when the maximum wind ahead of the trough is exporting positive vorticity and when the trough characterizes a more baroclinic nature (Reference 20).

It was noted by Palmen and Newton (Reference 1) that during the preocclusion stage when the jet maximum core is ahead of the trough, the cyclonic vorticity from both the curvature and shear effect from the jet is no longer being advected into the trough. It is this cyclonic vorticity that produces kinetic energy in the upper troposphere needed to sustain enough vertical shear in order to keep the frontal zone bounding the cold air in equilibrium. Without this kinetic energy, the equilibrium between the solenoids in a vertical plane across the flow and the centrifugal and coriolis acceleration associated with the vertical shear are no longer in balance, and the front bounding the cold dome aloft collapses. The subsiding cold dome then moves toward lower latitudes and around the base and ahead of the trough following the jet maximum. It is the subsiding cold air that finally cuts off the extratropical

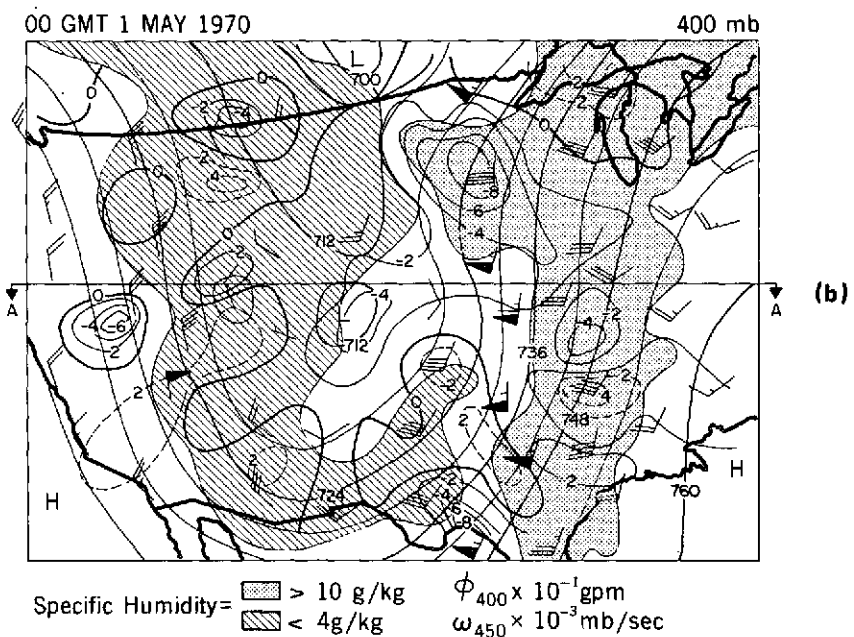
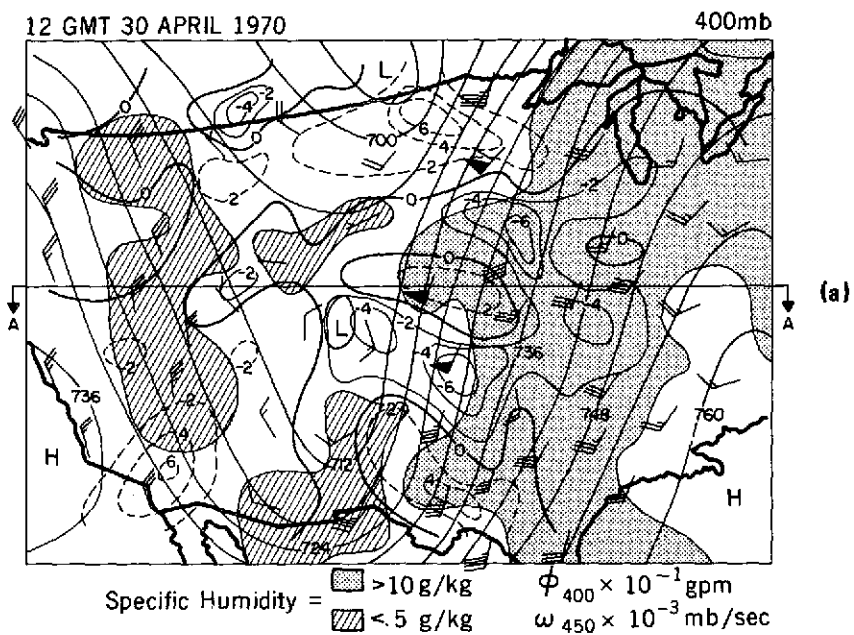


Figure 7. 400-mbar geopotential heights, and winds superimposed upon the 450-mbar vertical motion fields and the 500-mbar specific humidity fields over the Central United States for (a) 1200 GMT on April 30, and (b) 00 GMT on May 1. Line A designates location of cross section A. Positive vertical motion values represent downward motion.

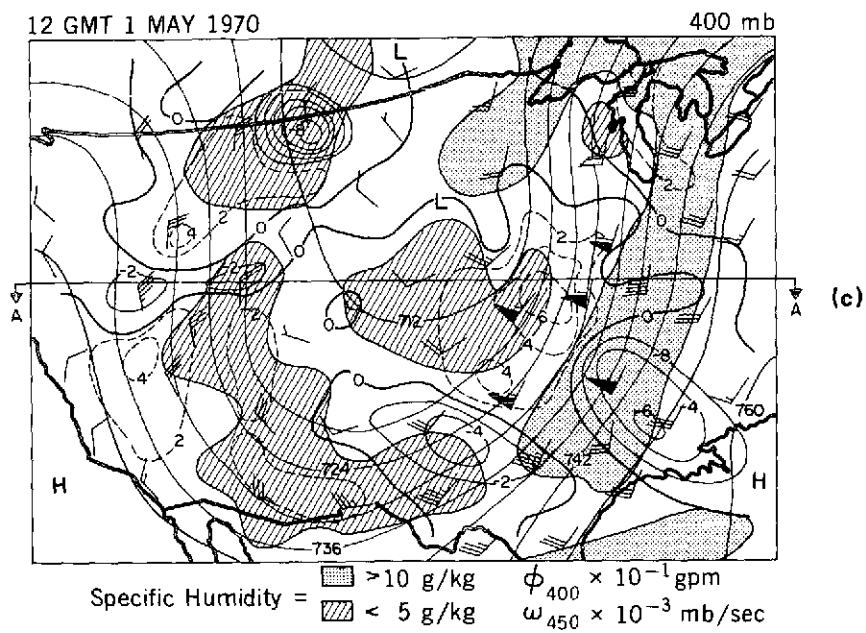


Figure 7. 400-mbar geopotential heights, and winds superimposed upon the 450-mbar vertical motion fields and the 500-mbar specific humidity fields over the Central United States for (c) 1200 GMT on May 1, 1970. Line A designates location of cross section A. Positive vertical motion values represent downward motion.

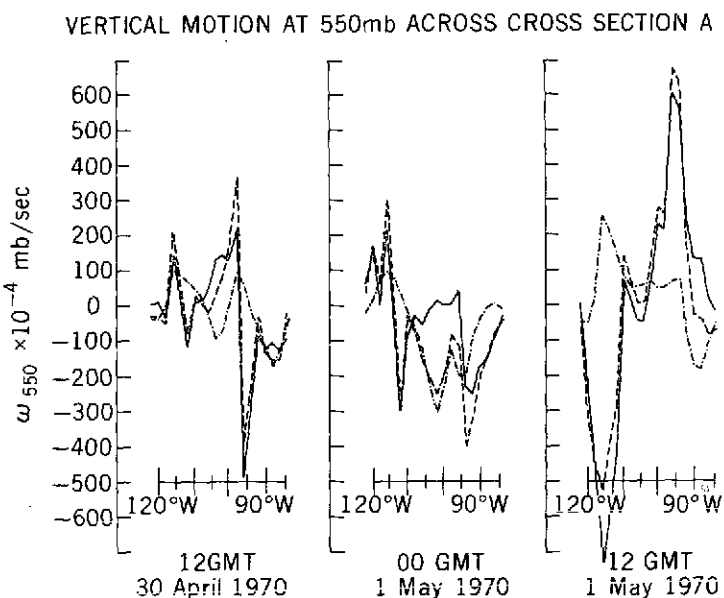


Figure 8. Partitioned and total quasi-geostrophic vertical velocities at 550 mb along cross section A at 1200 GMT on April 30, 00 GMT on May 1, and 1200 GMT on May 1, 1970, where the dash lines represent thermal contribution, dash-dot lines represent vorticity contribution, and the solid lines represent total contribution.

cyclone moisture supply during the occlusion stage of the trough's development. It is these conditions that are seen in this case study.

As seen in Figure 7(a), the area subsiding at the rate of 4×10^{-3} mbar/s that was seen entering West Texas at 1200 GMT on April 30, 1970, corresponds to the leading edge of the dry tongue. From the calculated and partitioned values of the total vertical motion, it is determined that this descending motion was induced mainly by the Laplacian of horizontal advection of cold air that was once part of the collapsing cold dome delineated by the large area of subsidence in the southwest corner of the trough. Differential negative vorticity advection created by the anticyclonic shearing on the cyclonic side of the existing jet maximum also contributed to subsidence. Thus, the dry cold air entering the eastern part of the trough created subsidence in advance of the dry tongue, which further enhanced the drying process.

This subsidence is depicted by trajectory 2 in Figure 6(a) during the first 3 hr. Twelve hours later at 00 GMT on May 1, 1970, the dry air had advanced northeastward, and the rate of subsidence in this area during the period had decreased to 2×10^{-3} mbar/s. The calculated partitioned value of the total vertical motion again suggested that the Laplacian of horizontal cold air advection had induced most of the subsidence. At 1200 GMT on May 1, 1970, the dry air had advanced into the Upper Mississippi Valley. The rate of subsidence had increased to values greater than 6×10^{-3} mbar/s. Although the Laplacian of horizontal cold air advection induced most of the subsidence, the differential negative vorticity advection produced by the existing jet maximum enhanced the subsidence. This increase in subsidence during the last 12 hr of the period is shown in trajectory 3 of Figure 6(b).

The ascending motion seen in trajectory 1 during the entire 24-hr period as shown in Figures 6(a) and (b) represents the area of upward vertical motion of more than -4×10^{-3} mbar/s, seen at both 1200 GMT on April 30, and 00 GMT on May 1, 1970, in Figures 7(a) and (b). This ascending motion was induced by the differential positive vorticity advection caused by the cyclonic curving circulation around the secondary closed low. The ascending air parcel seen east of the jet maximum in trajectories 3, 4, and 5 in Figure 6(a) and in 4 and 5 in Figure 6(b) were all caused by a large area of upward vertical motion induced by both differential positive vorticity advection created by the jet maximum and the Laplacian of horizontal warm air advection.

To examine the vertical extent of these areas of vertical motion, a cross section was made across the grid. The cross section intersected the same sector as cross section A' did, but extended further west to intersect the whole trough. Line A in Figures 7(a), (b), and (c) delineate this cross section. Figures 9(a), (b), and (c) depict cross section A at 1200 GMT on April 30, 00 GMT on May 1, and 1200 GMT on May 1, 1970, respectively. These figures show the vertical motions, the polar jet location as it intersects the cross section designated by J, and specific humidity patterns for a layer from 800 mbar to 100 mbar. During the period at about 98° W longitude, where the dry tongue traversed the cross section, the middle tropospheric subsidence area of 1200 GMT on April 30, 1970, had been

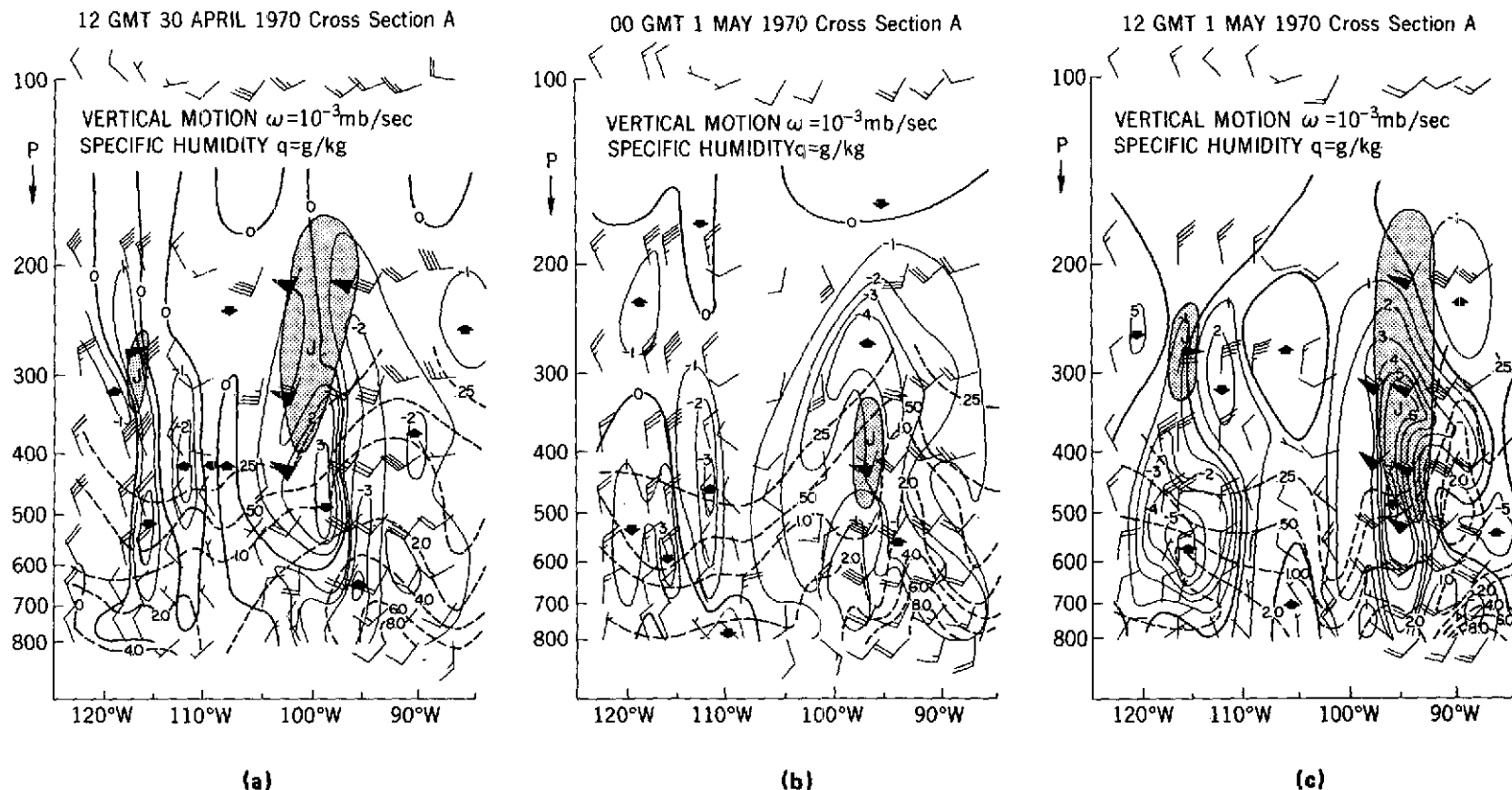


Figure 9. Cross section A showing from the 800- to 100-mbar level the specific humidity in dash lines, vertical motion in solid lines, and wind velocity and direction for (a) 1200 GMT on April 30, (b) 00 GMT on May 1, and (c) 1200 GMT on May 1, 1970. Positive vertical motion values represent downward motion.

replaced 12 hr later by the large area of ascending motion seen in Figure 7(b). However, in this area of ascending motion at 00 GMT on May 1, 1970, the area of dryness seen in the middle troposphere is maintained by horizontal advection from upstream. It was not until 1200 GMT on May 1, 1970, that there was evidence of further subsidence. In Figure 7(c), this subsidence is seen entering the cross section at 95° W longitude over the Upper Mississippi Valley. This subsidence at a rate greater than 6×10^{-3} mbar/s extended through the upper as well as the middle troposphere and explained the area of very warm T_{BB} 's greater than 255 K seen at 38° N latitude and 95° W longitude in Figure 4(c).

The subsiding cold dome behind the trough was between 110° W and 120° W longitude during the 24-hr period. Since the cross section did not intersect the southwest corner of the trough, the large subsidence created by the collapsing cold dome was not seen.

It is now evident what is being seen in the water vapor radiometric data. The radiometric data followed the movement of the denser air in the upper and middle troposphere that was once a part of the cold dome behind the trough, as it subsided, dried, and infiltrated the eastern portion of the trough.

CONCLUSIONS

This study has attempted to provide a more definitive basis for interpreting radiometrically observed $6.7\text{-}\mu\text{m}$ observations to infer dynamics in the middle and upper troposphere. In this case study it was found that changes in the shape and the magnitude of warm T_{BB} configurations in the water vapor data do delineate significant upper and middle tropospheric dynamical features. In particular, it was observed that the configuration in the water vapor radiometric data best reflected three-dimensional advection processes in areas where T_{BB} was greater than 245 K. It was found that subsidence is occurring in these areas but that the changes in T_{BB} are being produced mainly by horizontal advection processes. Since this case study was very selective and by no means exhausted all upper and middle tropospheric dynamic possibilities, additional synoptic studies should be pursued in order to further substantiate these results. Studies that would be particularly appropriate would involve different stages of development of extratropical and tropical storms. With the aid of a water vapor channel onboard a geosynchronous satellite, it would seem quite possible to monitor mesoscale dynamics associated with severe local storms and thus aid in the forecasting of these phenomena.

ACKNOWLEDGMENTS

The authors wish to thank their colleagues in the Laboratory for Meteorology and Earth Sciences for many discussions on the utility of $6.7\text{-}\mu\text{m}$ observations. Particular gratitude is expressed to Dr. R. Wexler for a careful review and comments on the manuscript.

Goddard Space Flight Center
National Aeronautics and Space Administration
Greenbelt, Maryland, August 2, 1973
039-23-01-01-51

REFERENCES

1. Palmen, E., and C. W. Newton, *Atmospheric Circulation System*, Academic Press, New York and London, 1969, pp. 379-86, and pp. 341-44.
2. Reiter, E. R., *Atmosphere Transport Processes*, U. S. Atomic Energy Commission Division of Technical Information, 1971, pp. 65-72.
3. Moller, F., and E. Raschke, *Evaluation of TIROS III Radiation Data*, NASA Report No. CR-112 NASA, 1964, pp. 84.
4. Allison, L. J., and G. Warnecke, *The Interpretation of TIROS Radiation Data for Practical Use in Synoptic Weather Analysis*, NASA Technical Note D-2851, p. 28.
5. Raschke, E., and W. R. Bandeen, "A Quasi-Global Analysis of Troposphere Water Vapor Content from TIROS IV Radiation," *J. Appl. Meteor.*, 6, 1967, pp. 468-81.
6. Fritz, S., and P. K. Rao, "On the Infrared Transmission Through Cirrus Clouds and the Estimation of Relative Humidity from Satellites," *J. Appl. Meteor.*, 6, 1967, pp. 1088-96.
7. Smith, W. L., "An Improved Method for Calculating Tropospheric Temperature and Moisture from Satellite Radiometer Measurements," *Mo. Weather Review*, 96, 1968, pp. 387-96.
8. Smith, W. L., and H. B. Howell, "Vertical Distribution of Water Vapor from Satellite Infrared Spectrometer Measurements," *J. Appl. Meteor.*, 10, 1971, pp. 1026-34.
9. Hanel, R. A., and B. J. Conrath, "Thermal Emission Spectra of the Earth and Atmosphere from the Nimbus-4 Michelson Interferometer Experiment," *Nature*, 228, 1970, pp. 143-45.
10. Nordberg, W., A. W. McCulloch, L. L. Foshee, and W. R. Bandeen, "Preliminary Results from Nimbus II," *Bull. American Meteor. Soc.*, 47, 1966, pp. 857-72.
11. Beran, D. W., E. S. Merrit, and D. T. Chang, *Interpretation of Baroclinic Systems and Wind Fields as Observed by Nimbus II MRIR*, Final Report 9643-F Allied Research Associates, Inc., 1968, p. 135.

12. Martin, F. L., and V. V. Salomonson, "Statistical Characteristics of Subtropical Jet Stream Features in Terms of MRIR Observations from Nimbus-2," *J. Appl. Meteor.*, 9, 1970, pp. 508-20.
13. Steranka, J., L. J. Allison, and V. V. Salomonson, "Application of Nimbus-4 THIR 6.7- μ m Observation to Regional and Global Moisture and Wind Field Analyses," *J. Appl. Meteor.*, 12, 1973, pp. 386-95.
14. Holub, R. J., and W. E. Shenk, *A Multispectral Study of an Extratropical Cyclone with Nimbus-3 THIR Data*, NASA Technical Note D-7184, 1973, p. 71.
15. Allison, L. J., J. Steranka, G. T. Cherrix, and E. Hilsenrath, "Meteorological Application of Nimbus-4 Temperature-Humidity Infrared Radiometer, 6.7- μ m Channel Data," *Bull. American Meteor. Soc.*, 53, 1972, pp. 526-35.
16. McCulloch, A. W., "The Temperature-Humidity Infrared Radiometer (THIR) Experiment," *The Nimbus IV User Guide*, 1970, pp. 25-63.
17. Barr, S., P. E. Long, and I. A. Miller, *Atmospheric Sensing and Prediction Project*, Scientific Report No. 2, Air Force Cambridge Research Laboratories, 1970, p. 28.
18. Barr, S., W. K. Widger, Jr., I. A. Miller, and R. Stanton, "Objective Subsynoptic Upper Level Analysis," *J. Appl. Meteor.*, 10, 1971, pp. 410-17.
19. Rogers, C. W., and P. E. Sherr, *A Study of Dynamical Relationships Between Cloud Patterns and Extratropical Cyclogenesis*, Final Report E-47-67(), Allied Research Associates, Inc., 1967, p. 74.
20. Krishnamurti, T. N., "A Study of a Developing Wave Cyclone," *Mo. Weather Review*, 96, 1968, pp. 208-27.

SOURCES

Rodgers, E. B., and V. V. Salomonson, "A Quantitative Evaluation of the Nimbus Water Vapor Observations as Related to Middle and Upper Tropospheric Circulation Features," paper presented at the Fall Annual Meeting of American Geophys. Union, San Francisco, CA 6-9, December 1971.

Rodgers, E. B., and V. V. Salomonson, "Upper Tropospheric Dynamics as Reflected in Nimbus 4 THIR 6.7- μ m Data," paper presented at the Spring Annual Meeting of American Geophys. Union, Washington, D. C., April 16-20, 1973.

Shenk, W. E., and E. B. Rodgers, *Satellite Radiometric Views of Hurricane Camille*, NASA Technical Note, to be published.

Shenk, W. E., and V. V. Salomonson, "Visible and Infrared Imagery from Meteorological Satellites," *Applied Optics*, 9, 1970, pp. 1747-60.

Steranka, J., L. J. Allison, and V. V. Salomonson, "Improvement of Synoptic Scale Moisture and Wind Field Analysis Using the Nimbus-4 THIR 6.7- μ m Observations," NASA X-651-72-101, 1972.